

# High-order dynamical decoupling in the weak-coupling regime

Leeseok Kim<sup>1</sup> and Milad Marvian<sup>1</sup>

<sup>1</sup>*Center for Quantum Information and Control and Department of Electrical and Computer Engineering, University of New Mexico, NM 87131, USA*

We introduce a high-order dynamical decoupling (DD) scheme for arbitrary system-bath interactions in the weak-coupling regime. Given any decoupling group  $\mathcal{G}$  that averages the interaction to zero, our construction yields pulse sequences whose length scales as  $\mathcal{O}(|\mathcal{G}|K)$ , while canceling all error terms linear in the system-bath coupling strength up to order  $K$  in the total evolution time. As a corollary, for an  $n$ -qubit system with  $k$ -local system-bath interactions, we obtain an  $\mathcal{O}(n^{k-1}K)$ -pulse sequence, a significant improvement over existing schemes with  $\mathcal{O}(\exp(n))$  pulses (for  $k = \mathcal{O}(1)$ ). The construction is obtained via a mapping to the continuous necklace-splitting problem, which asks how to cut a multi-colored interval into pieces that give each party the same share of every color. We provide explicit pulse sequences for suppressing general single-qubit decoherence, prove that the pulse count is asymptotically optimal, and verify the predicted error scaling in numerical simulations. For the same number of pulses, we observe that our sequences outperform the state-of-the-art Quadratic DD in the weak-coupling regime. We also note that the same construction extends to suppress slow, time-dependent Hamiltonian noise.

Dynamical decoupling (DD) [1] is a powerful technique for mitigating decoherence caused by unavoidable system-bath interactions. The central idea is to apply a sequence of fast control pulses to the system, effectively averaging out the coupling between the system and its environment. Due to its effectiveness and relatively low overhead, DD has been extensively explored both theoretically [2–22] and experimentally [23–39] across a wide range of platforms, making it a key ingredient in the implementation of state-of-the-art quantum processors [40–45].

Since the 1950s, numerous DD sequences have been proposed to suppress decoherence more effectively. These designs typically aim to increase the cancellation order in the total evolution time  $T$ , but at the cost of more number of pulses. For the most general case of single-qubit system-bath coupling, two high-order DD protocols have been developed. The earliest is Concatenated DD (CDD) [7], whose number of pulses grows exponentially with the cancellation order  $K$ . This was followed by Quadratic DD (QDD) [13] which achieves the same decoupling order while requiring only a quadratic number of pulses in  $K$ .

For  $n$ -qubit systems, both CDD and the multi-qubit generalization of QDD, Nested Uhrig DD (NUDD) [17, 18], can suppress fully general decoherence. However in many physical settings the dominant noise is  $k$ -local (often with a constant  $k$ ), meaning it affects only a small subset of qubits at a time [16, 46–48]. In this case, first-order DD sequences based on orthogonal arrays (OA) have been constructed whose pulse count scales as  $\mathcal{O}(n^{k-1})$  and therefore explicitly reflects the noise locality [20]. To date, however, there is no high-order DD construction that exploits the  $k$ -local structure of the noise. While CDD and NUDD apply to  $k$ -local models as well, they do not take the locality parameter  $k$  into account and thus substantially overestimate the required number

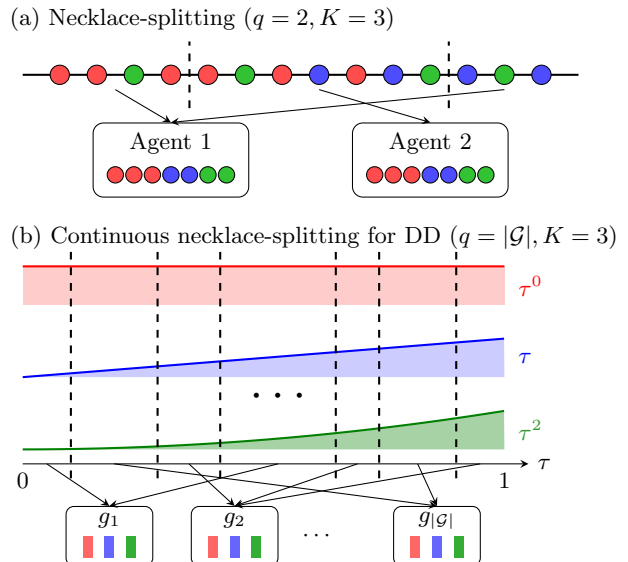


FIG. 1: (a) Discrete necklace-splitting example with two agents ( $q = 2$ ) and three colors ( $K = 3$ ): by choosing two cuts, each agent receives the same number of red, blue, and green beads. (b) Continuous necklace-splitting picture for dynamical decoupling: the first three time-moments  $\int_0^1 \tau^m d\tau$  ( $K = 3$  in this example) are partitioned by the cuts and assigned to the  $|\mathcal{G}|$  agents ( $q = |\mathcal{G}|$ ) so that each agent receives the same moments. In the DD construction, the cuts mark the pulse times,  $\mathcal{G}$  denotes the decoupling group for the given noise model, and the time-moments correspond to the error terms, whose equal distribution ensures that averaging over the group cancels these contributions. The necklace-splitting theorem guarantees that there exist at most  $(q - 1)K$  such cuts.

of pulses.

In this Letter, we present a high-order DD con-

Scheme	System / noise model	Leading error scaling	Number of pulses
<b>Single-qubit, general noise</b>			
CDD [7]	1-qubit, general	$\mathcal{O}(JT^{K+1}) + \mathcal{O}(J^2T^2)$	$\mathcal{O}(4^K)$
QDD [13]	1-qubit, general	$\mathcal{O}(JT^{K+1}) + \mathcal{O}(J^2T^{K+1})$	$\mathcal{O}(K^2)$
This work	1-qubit, general	$\mathcal{O}(JT^{K+1}) + \mathcal{O}(J^2T^2)$	$\mathcal{O}(K)$
<b><math>n</math>-qubit, general noise</b>			
CDD [7]	$n$ qubits, general	$\mathcal{O}(JT^{K+1}) + \mathcal{O}(J^2T^2)$	$\mathcal{O}(4^{nK})$
NUDD [17, 18]	$n$ qubits, general	$\mathcal{O}(JT^{K+1}) + \mathcal{O}(J^2T^{K+1})$	$\mathcal{O}(K^{2n})$
This work	$n$ qubits, general	$\mathcal{O}(JT^{K+1}) + \mathcal{O}(J^2T^2)$	$\mathcal{O}(4^n K)$
<b><math>n</math>-qubit, <math>k</math>-local noise</b>			
OA-based DD [20]	$n$ qubits, $k$ -local	$\mathcal{O}(JT^2) + \mathcal{O}(J^2T^2)$	$\mathcal{O}(n^{k-1})$
This work	$n$ qubits, $k$ -local	$\mathcal{O}(JT^{K+1}) + \mathcal{O}(J^2T^2)$	$\mathcal{O}(n^{k-1}K)$

TABLE I: Comparison of representative dynamical decoupling (DD) schemes, showing the noise model, leading error scaling, and pulse-count scaling as functions of cancellation order  $K$ , system size  $n$ , and noise locality  $k$ . Abbreviations: CDD = Concatenated DD, QDD = Quadratic DD, NUDD = Nested Uhrig DD, OA = orthogonal-array. Our construction cancels all contributions linear in the system-bath coupling strength  $J$  up to order  $K$  in the total evolution time  $T$  using a number of pulses linear in  $K$ , and applies to any noise model admitting a decoupling group  $\mathcal{G}$ . In particular, there exist choices of  $\mathcal{G}$  with size  $\mathcal{O}(1)$  for general single-qubit noise,  $\mathcal{O}(4^n)$  for general  $n$ -qubit noise, and  $\mathcal{O}(n^{k-1})$  for  $k$ -local noise on  $n$  qubits.

struction for arbitrary system-bath interactions in the weak-coupling regime, where the system-bath interaction strength is small compared with the intrinsic system and/or the bath energy scales (defined more precisely later), a condition that is well motivated in many physical platforms [49]. This regime is standard in the DD literature, with typical benchmarks assuming coupling  $10^{-2}$ – $10^{-6}$  times the pure-bath energy scale [7, 12–16, 19, 22]. DD is also widely used to preserve the system’s intended dynamics while suppressing weaker couplings to the environment—for instance, to maintain a desired system evolution to perform robust quantum computation [12, 16, 35, 50–54] or to preserve the sensing signal [55].

Our scheme yields pulse sequences whose length scales linearly with both the cancellation order  $K$  and decoupling group size  $|\mathcal{G}|$ , while cancelling all error terms are linear in the system-bath coupling strength  $J$  up to order  $K$  in the total evolution time  $T$ . In the weak-coupling regime, where these first-order in  $J$  contributions dominate the error, our sequences (1) achieve the same leading-order scaling  $\mathcal{O}(JT^{K+1})$  as CDD, QDD, and NUDD for single-qubit and general  $n$ -qubit decoherence, but with substantially fewer pulses, and (2) provide, to our knowledge, the first high-order DD construction for  $k$ -local noise whose pulse complexity explicitly reflects the locality, scaling as  $\mathcal{O}(n^{k-1}K)$ . These results are summarized in Table I. In particular, for single-qubit general decoherence we match the leading error scaling of QDD using only  $\mathcal{O}(K)$  pulses, and we further prove that this linear scaling is asymptotically optimal. Outside this

weak-coupling regime, however, the residual second-order contribution in our scheme scales only as  $J^2T^2$ . Hence, protocols such as QDD and NUDD, which suppress all higher-order terms in  $T$  at every order in  $J$ , can outperform our construction in the strong-noise regime.

We first show that a pulse sequence of length at most  $(|\mathcal{G}| - 1)K$  must exist. We demonstrate this by relating the pulse-scheduling task to the necklace-splitting problem [56], introduced in the 1980s and widely studied in fair division and combinatorics. In its simplest form, the necklace-splitting problem asks: given a necklace with beads of several colors, can one cut the necklace into pieces and distribute them among a fixed number of players so that each player receives exactly the same quantity of every color? This fair-division framework provides a natural abstraction for our construction: the different bead colors correspond to different cancellation conditions that the DD sequence must satisfy, while assigning pieces to players corresponds to choosing the appropriate toggling (or pulse) operators (see Figure 1). Moreover, by leveraging known efficient approximation algorithms for the necklace-splitting problem [57], such sequences can be constructed explicitly in  $\mathcal{O}(\text{poly}(|\mathcal{G}|, K))$  time. Finally, we numerically obtain explicit DD pulse sequences of length  $3K$  for 1-local noise model and confirm their error scaling through simulations. We find that, in the weak-coupling regime, our sequences can outperform QDD using the same number of pulses.

*Setting and notation.*— We consider an  $n$ -qubit system

$S$  coupled to a bath  $B$  with

$$H(t) = H_S \otimes I_B + I_S \otimes H_B + H_{SB} + H_c(t) \otimes I_B, \quad (1)$$

where  $H_S$  is the internal system Hamiltonian,  $H_B$  is the bath Hamiltonian,  $H_{SB}$  describes the interaction between the system and the bath, and the control Hamiltonian  $H_c(t)$ .

We expand the interaction as  $H_{SB} = \sum_{\alpha} \sigma_{\alpha} \otimes B_{\alpha}$ , where  $\sigma_{\alpha}$  are (non-identity)  $n$ -qubit Pauli strings and  $B_{\alpha}$  are Hermitian bath operators. We assume the norm bounds

$$\|H_0\| \leq \beta, \quad \sum_{\alpha} \|B_{\alpha}\| \leq J, \quad (2)$$

and set  $\beta = 1$  (so in physical units  $T \mapsto \beta T$  and  $J \mapsto J/\beta$ ).

Control is modeled as instantaneous Pauli pulses on  $S$ : at times  $0 < t_1 < \dots < t_L < T$  we apply  $P_j$ , yielding the piecewise-constant propagator  $U_c(t) = P_j \dots P_1$  for  $t \in [t_j, t_{j+1})$  with  $U_c(0) = I_S$ . Following the standard design assumption that  $[H_0, H_c(t)] = 0$  (see the definition of the decoupling group (14)), the reference evolution is  $U_0(t) = U_c(t)e^{-iH_0t}$ , and the total propagator can be written as

$$U(t) = U_0(t)\mathcal{T} \exp\left(-i \int_0^t \tilde{H}(t')dt'\right), \quad (3)$$

where  $\tilde{H}(t) := U_0^\dagger(t)H_{SB}U_0(t)$ .

Using  $U_0(t) = U_c(t)e^{-iH_0t}$  and  $H_{SB} = \sum_{\alpha} \sigma_{\alpha} \otimes B_{\alpha}$ , the toggling-frame Hamiltonian is

$$\tilde{H}(t) = \sum_{\alpha} e^{iH_0t} (U_c^\dagger(t)\sigma_{\alpha}U_c(t) \otimes B_{\alpha}) e^{-iH_0t}. \quad (4)$$

Since  $U_c(t)$  is a piecewise-constant Pauli operator, for each  $\alpha$  we define  $y_{\alpha}(t) \in \{\pm 1\}$  by  $U_c^\dagger(t)\sigma_{\alpha}U_c(t) = y_{\alpha}(t)\sigma_{\alpha}$ . Hence,

$$\tilde{H}(t) = \sum_{\alpha} y_{\alpha}(t)e^{iH_0t} (\sigma_{\alpha} \otimes B_{\alpha}) e^{-iH_0t}, \quad (5)$$

where the switching functions  $\{y_{\alpha}(t)\}$  are fixed by the pulse sequence.

*Error target and generalized moment conditions.*— Our goal is to choose switching functions  $y_{\alpha}(t) \in \{\pm 1\}$  such that

$$\|U(T) - U_0(T)\| = \mathcal{O}(JT^{K+1}) + \mathcal{O}(J^2T^2). \quad (6)$$

We call the *weak-coupling* regime the parameter range where the linear-in- $J$  term dominates, i.e.  $J = \mathcal{O}(T^{K-1})$  (before setting  $\beta = 1$ , this is  $J/\beta = \mathcal{O}((\beta T)^{K-1})$ ).

Write  $U(T) = U_0(T)U_I(T)$  with  $U_I(T) = \mathcal{T} \exp\left(-i \int_0^T \tilde{H}(t)dt\right)$ . Assuming Magnus convergence

(e.g.  $JT < \pi$ ) [58, 59], we expand  $U_I(T) = \exp(\sum_{m \geq 1} \Omega_m(T))$ , where

$$\Omega_1(T) = -i \int_0^T \tilde{H}(t)dt, \quad (7)$$

$$\Omega_2(T) = -\frac{1}{2} \int_0^T dt_1 \int_{t_1}^{t_2} dt_2 [\tilde{H}(t_1), \tilde{H}(t_2)]. \quad (8)$$

Using Eq. (2), we obtain  $\|\Omega_2(T)\| = \mathcal{O}(J^2T^2)$ . Thus,

$$U(T) = U_0(T) (I + \Omega_1(T) + \mathcal{O}(J^2T^2)). \quad (9)$$

It therefore suffices to engineer  $\|\Omega_1(T)\| = \mathcal{O}(JT^{K+1})$ , which implies Eq. (6).

To characterize  $\Omega_1$ , expand  $e^{iH_0t}(\sigma_{\alpha} \otimes B_{\alpha})e^{-iH_0t} = \sum_{m=0}^{\infty} \frac{i^m}{m!} \text{ad}_{H_0}^m(\sigma_{\alpha} \otimes B_{\alpha})t^m$ . Defining the dimensionless parameter  $\tau = t/T$ ,

$$\Omega_1(T) = -i \sum_{\alpha} \int_0^T y_{\alpha}(t)e^{iH_0t}(\sigma_{\alpha} \otimes B_{\alpha})e^{-iH_0t}dt, \quad (10)$$

$$= -i \sum_{\alpha} \sum_{m=0}^{\infty} C_{\alpha,m} M_{\alpha,m} T^{m+1}, \quad (11)$$

where  $C_{\alpha,m} := \frac{i^m}{m!} \text{ad}_{H_0}^m(\sigma_{\alpha} \otimes B_{\alpha})$  are independent of time and  $y_{\alpha}$ , and the generalized moments are defined as

$$M_{\alpha,m} \equiv \int_0^1 y_{\alpha}(\tau) \tau^m d\tau. \quad (12)$$

Thus  $\Omega_1(T)$  begins at order  $T^{K+1}$  if and only if

$$M_{\alpha,m} = 0 \quad (m = 0, 1, \dots, K-1, \forall \alpha \text{ in } H_{SB}), \quad (13)$$

which, together with Eq. (2), yields the scaling in Eq. (6).

*Main result.*— Let  $\mathcal{G} \subset \mathcal{P}_n$  be a finite subgroup of the  $n$ -qubit Pauli group. We say  $\mathcal{G}$  is a *decoupling group* [1, 22, 60] for  $H$  if every element commutes with the system Hamiltonian  $H_S$  (equivalently, with  $H_0$ ) and the group twirl of the system-bath interaction vanishes:

$$\forall g \in \mathcal{G}, \quad [H_0, g \otimes I_B] = 0, \quad \Pi_{\mathcal{G}}(H_{SB}) = 0, \quad (14)$$

$$\text{where } \Pi_{\mathcal{G}}(X) := \frac{1}{|\mathcal{G}|} \sum_{g \in \mathcal{G}} (g^\dagger \otimes I_B) X (g \otimes I_B).$$

Our central result shows that the order- $K$  moment constraints in Eq. (13) can always be met using at most  $(|\mathcal{G}| - 1)K$  pulses.

**Theorem 1** (Existence of an order- $K$  moment-cancelling sequence with at most  $(|\mathcal{G}| - 1)K$  pulses). *Let  $H = H_0 + H_{SB}$  with  $H_{SB} = \sum_{\alpha} \sigma_{\alpha} \otimes B_{\alpha}$  and let  $\mathcal{G}$  be a decoupling group for  $H$  as defined in Eq. (14). For any integer  $K \geq 1$ , there exist piecewise-constant functions  $y_{\alpha} : [0, 1] \rightarrow \{\pm 1\}$ , indexed by all Pauli strings  $\sigma_{\alpha}$  appearing in  $H_{SB}$ , such that:*

1. there exist (normalized) pulse timings  $0 < \tau_1 < \dots < \tau_L < 1$  with

$$L \leq (|\mathcal{G}| - 1)K \quad (15)$$

for which all  $y_\alpha(\tau)$  are constant on each subinterval  $[0, \tau_1), [\tau_1, \tau_2), \dots, [\tau_L, 1]$ , and

2. the generalized moments in (12) vanish,

$$M_{\alpha, m} = \int_0^1 y_\alpha(\tau) \tau^m d\tau = 0, \quad (16)$$

for all  $\alpha$  and all  $m = 0, 1, \dots, K - 1$ .

The full proof of Theorem 1 is provided in the Supplemental Material (SM). Here we give the intuition and explain the role of necklace splitting. View normalized time  $\tau \in [0, 1]$  as a continuous necklace whose point  $\tau$  carries  $K$  “colors” with weights  $1, \tau, \dots, \tau^{K-1}$  (cf. Fig. 1 (b)). The continuous necklace-splitting theorem [56] (Lemma S2 in SM) guarantees that with at most  $(|\mathcal{G}| - 1)K$  cuts we can distribute the pieces among  $|\mathcal{G}|$  bins labeled by  $g \in \mathcal{G}$  so that every bin receives exactly the same amount of every color. Assigning to each bin the corresponding toggling-frame sign pattern (from conjugation by  $g$ ) makes all low-order time weights identical across bins, and the decoupling-group condition implies these signed contributions sum to zero. Hence all moments up to order  $K - 1$  vanish.

Given a labeled partition  $0 = t_0 < t_1 < \dots < t_L < t_{L+1} = T$  with segment labels  $g_\ell \in \mathcal{G}$  ( $\ell = 0, \dots, L$ ) and  $g_0 = I$ , the physical pulse sequence is

$$P_\ell := g_\ell g_{\ell-1}^\dagger, \quad (17)$$

so that  $U_c(t) = g_\ell$  for  $t \in [t_\ell, t_{\ell+1})$ .

Given  $K$  nonnegative continuous functions  $f_1, \dots, f_K : [0, 1] \rightarrow [0, \infty)$  and an integer  $q \geq 2$ , an  $\varepsilon$ -consensus splitting is a partition of  $[0, 1]$  into at most  $L + 1$  subintervals together with an assignment of each subinterval to one of  $q$  bins  $A_1, \dots, A_q$  such that, for every  $j \in [K]$  and  $c \in [q]$ ,

$$\left| \int_{A_c} f_j(\tau) d\tau - \frac{1}{q} \int_0^1 f_j(\tau) d\tau \right| \leq \frac{\varepsilon}{q} \int_0^1 f_j(\tau) d\tau. \quad (18)$$

A natural goal is to minimize the number of cuts  $L$ , but this is computationally difficult in general. Already for  $q = 2$ , for some fixed constant  $\varepsilon_0 > 0$  it is NP-hard to even decide whether an  $\varepsilon_0$ -consensus splitting exists using  $K - 1$  cuts [61], which is only one less than the  $K$  cuts for which existence is guaranteed by the continuous necklace-splitting theorem (Lemma S2 in the SM). However, if one allows a modest overhead in the cut budget, efficient constructions become possible. In fact, there exists an efficient deterministic offline algorithm [57] which, given oracle access to the  $K$  measures, computes the cut positions using at most

$$L \leq (q - 1)K \left[ 2 + \log_2 \frac{3q}{\varepsilon} \right] \quad (19)$$

cuts with  $\mathcal{O}(\text{poly}(q, K, \log(1/\varepsilon)))$  runtime. In our setting ( $q = |\mathcal{G}|$ ,  $f_m(\tau) = \tau^m$ ,  $m = 0, \dots, K-1$ ), labeling bins by  $g_c \in \mathcal{G}$  as in the proof of Theorem 1 yields a constructive protocol with  $L \leq (|\mathcal{G}| - 1)K \left[ 2 + \log_2 \frac{3|\mathcal{G}|}{\varepsilon} \right]$  pulses and  $|M_{\alpha, m}| = \left| \int_0^1 y_\alpha(\tau) \tau^m d\tau \right| \leq \varepsilon \int_0^1 \tau^m d\tau = \frac{\varepsilon}{(m+1)}$ , for all  $\alpha$  and  $m = 0, 1, \dots, K - 1$ .

*Implication:  $k$ -local noise model.*— Suppose that  $H_{SB}$  is  $k$ -local, in the sense that every Pauli term  $\sigma_\alpha$  appearing in  $H_{SB}$  has weight at most  $k$ . In this setting, one can construct decoupling group  $\mathcal{G}$  of size  $|\mathcal{G}| = \mathcal{O}(n^{k-1})$  [20]. Theorem 1 guarantees the existence of pulse sequences with length

$$L = \mathcal{O}(n^{k-1} K), \quad (20)$$

for which  $M_{\alpha, m} = 0$  for all  $m = 0, 1, \dots, K - 1$  and all Pauli strings  $\sigma_\alpha$  of weight at most  $k$ . To the best of our knowledge, this is the first construction of high-order DD sequences whose pulse count explicitly reflects the locality of the noise, in contrast to generic high-order schemes such as CDD [7] and NUDD [18], whose cost does not exploit  $k$ -local structure. For  $k = \mathcal{O}(1)$ , our DD uses  $\mathcal{O}(\text{poly}(n))$  pulses, whereas CDD and NUDD use  $\mathcal{O}(\exp(n))$  pulses; thus exploiting locality yields an exponential improvement.

For 1-local noise, the best-known sequence is QDD [13], which achieves error suppression of order  $\mathcal{O}(JT^{K+1}) + \mathcal{O}(J^2T^{K+1})$  using  $\mathcal{O}(K^2)$  pulses. Consequently, in the weak-coupling regime where the  $\mathcal{O}(J)$  term dominates, our construction that uses only  $\mathcal{O}(K)$  pulses provides a quadratic reduction in the required number of pulses. Moreover, this linear scaling in  $K$  is optimal: any DD sequence satisfying  $M_{\alpha, m} = 0$  for all  $\alpha$  and  $m = 0, \dots, K - 1$  must use at least  $K$  pulses.

**Lemma 2** ( $\Omega(K)$  lower bound). *Let  $y : [0, 1] \rightarrow \{\pm 1\}$  be piecewise constant with  $r$  sign changes on  $(0, 1)$ . If*

$$\int_0^1 y(\tau) \tau^m d\tau = 0 \quad (m = 0, 1, \dots, K - 1), \quad (21)$$

*then necessarily  $r \geq K$ .*

The proof of Lemma 2 is provided in the SM. Since single-axis noise is a special case of general noise, the same lower bound applies here, and thus the  $\mathcal{O}(K)$  pulse scaling is optimal.

*Extension to slow, time-dependent Hamiltonian noise.*— Environmental fluctuations can be modeled as time-dependent Hamiltonian noise and suppressed by DD [26, 31, 32, 62, 63]. For a single qubit general noise,

$$H(t) = \sum_{\alpha \in \{x, y, z\}} \beta_\alpha(t) \sigma_\alpha + H_c(t), \quad (22)$$

where  $\beta_\alpha(t)$  are unknown time-dependent noise coefficients and  $H_c(t)$  is the control Hamiltonian that applies Pauli pulses. Expanding  $\beta_\alpha(t)$  in time, the leading

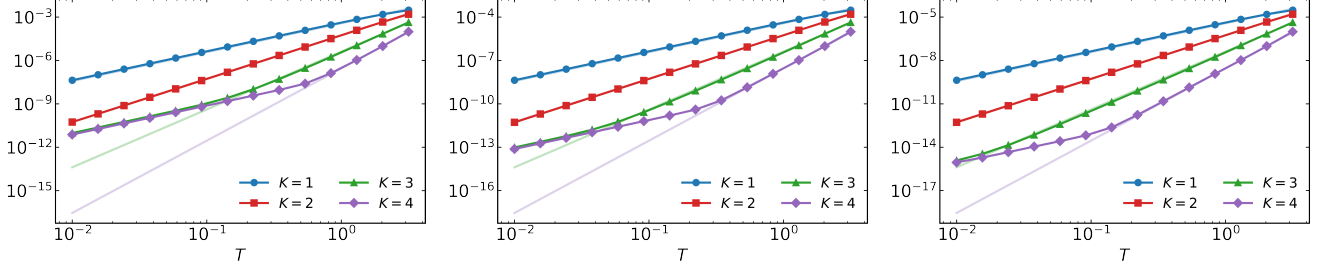


FIG. 2: Errors for optimized DD sequences at different coupling strengths (from left to right):  $J = 10^{-3}$ ,  $J = 10^{-4}$ , and  $J = 10^{-5}$ . Here  $\beta = 1$ , and  $T$  denotes the total evolution time. As  $J$  decreases, the error scaling increasingly follows the expected order  $K$  (indicated by shaded lines). A crossover is observed where the slope transitions from  $K$  to 2, consistent with the scaling  $\mathcal{O}(JT^{K+1}) + \mathcal{O}(J^2T^2)$ .

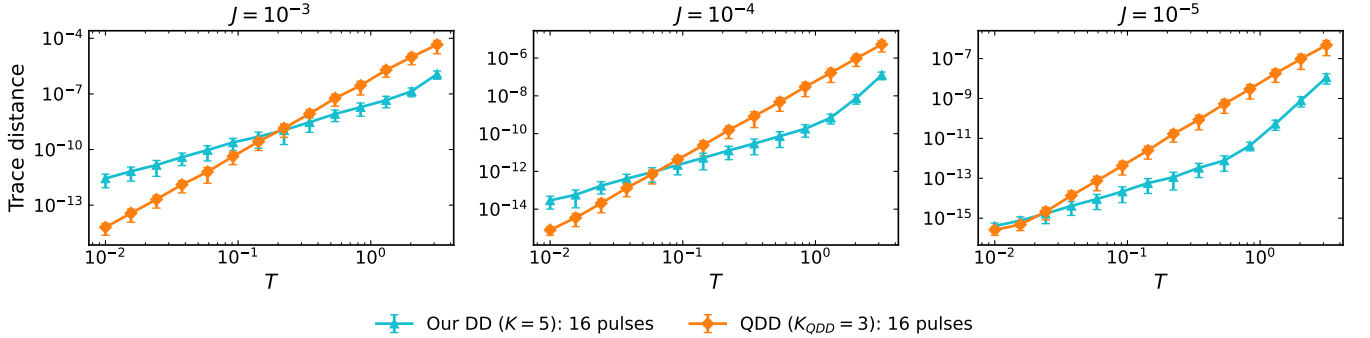


FIG. 3: Comparison between our DD sequences and QDD for the single-qubit general decoherence model. We show the average trace distance error of the reduced system state versus  $T$  for several small coupling strengths  $J$ , comparing our  $K = 5$  DD (16 pulses) with QDD at  $K_{\text{QDD}} = 3$  (16 pulses). We observe that our sequence achieves smaller errors as  $J$  decreases and for larger  $T$ , where higher-order cancellation is more effective. Each data point is averaged over 100 random initial product states.

toggling-frame Magnus term depends on the moments  $M_{\alpha,m}$ . Hence  $M_{\alpha,m} = 0$  for  $m = 0, \dots, K-1$  suppresses the leading error to order  $K$ . For slow (band-limited) noise with cutoff  $\omega_c$ , we obtain an error scaling of  $\|\tilde{U}(T) - I\| = \mathcal{O}(\beta_{\max} T(\omega_c T)^K) + \mathcal{O}(\beta_{\max}^2 T^2)$  where  $\beta_{\max} := \sup_{t \in [0, T]} \sum_{\alpha} |\beta_{\alpha}(t)|$ , which has the similar structure of the error scaling of Eq. (6). See the SM for details.

*Numerical simulation.*— We consider a single qubit with  $H_{SB} = \sum_{\alpha \in \{x, y, z\}} \sigma_{\alpha} \otimes B_{\alpha}$  and  $H_B = \sum_{\alpha \in \{x, y, z\}} c_{\alpha} \sigma_{\alpha}$ , with  $B_{\alpha} = \sum_{\mu \in \{x, y, z\}} c_{B_{\alpha}, \mu} \sigma_{\mu}$  and coefficients in  $[0, 1]$ . Here  $\mathcal{G} = \{I, X, Y, Z\}$ , so Theorem 1 gives an order- $K$  sequence with  $(|\mathcal{G}| - 1)K = 3K$  pulses. Imposing cyclicity  $U_c(T) = I$  may require one additional pulse at  $t = T$ , for a total of at most  $3K + 1$  pulses.

Although the efficient approximation algorithm yields at most  $(|\mathcal{G}| - 1)K \left[ 2 + \log_2 \frac{3|\mathcal{G}|}{\varepsilon} \right]$  pulses, the  $\log(1/\varepsilon)$  overhead can be large at the small error levels relevant for DD. In our single-qubit setting, the resulting schedules use roughly an order of magnitude more pulses than the existence bound  $L \leq 3K$  from Theorem 1.

We therefore determine the cut locations by direct numerical optimization: we fix  $L = 3K$  (i.e.,  $3K + 1$  segments) and restrict to an alternating pulse pattern  $X \rightarrow Z \rightarrow X \rightarrow Z \rightarrow \dots$ , which fixes the group traversal and hence  $y_{\alpha}(\tau) = \chi_{\alpha}(g(\tau))$ . Let  $\Delta\tau_1, \dots, \Delta\tau_L > 0$  with  $\sum_{\ell=1}^L \Delta\tau_{\ell} = 1$  denote the normalized inter-pulse intervals (the sign triple on each segment is then fixed by the chosen pattern). We choose  $\{\Delta\tau_{\ell}\}$  by minimizing the squared moment residuals up to order  $K - 1$ ,

$$\Phi(\Delta\tau) = \sum_{\alpha \in \{x, y, z\}} \sum_{m=0}^{K-1} \left| \int_0^1 y_{\alpha}(\tau; \Delta\tau) \tau^m d\tau \right|^2, \quad (23)$$

subject to the simplex constraint. We solve this constrained least-squares problem numerically; optimized schedules are reported in the SM. Our convention is free evolution on  $[0, \tau_1]$  followed by the first  $X$  pulse at  $t = \tau_1$  and the remaining pulses thereafter. For  $K = 1$ , the optimizer recovers XY4 [4].

We set  $H_S = 0$  and normalize  $\|H_B\| = \beta = 1$ . Following prior DD studies [7, 12–16, 19, 22], we take  $J \in \{10^{-3}, 10^{-4}, 10^{-5}\}$ . For each  $J$ , we plot the er-

ror  $\|U(T) - U_0(T)\|$  versus  $T$  using the numerically optimized schedules (see SM). The results are shown in Fig. 2. As  $J$  decreases, the scaling approaches the expected order- $K$  behavior (shaded guides). A crossover from slope  $K$  to 2 is observed, consistent with the prediction  $\mathcal{O}(JT^{K+1}) + \mathcal{O}(J^2T^2)$  in Eq. (6).

We next compare our sequence to QDD using the same number of pulses. Specifically, we benchmark our  $K = 5$  DD against QDD with  $K_{\text{QDD}} = 3$ , both of which use 16 pulses. For the same Hamiltonian model, we sample 100 random product initial states and plot the average trace distance between the reduced system state and the ideal reduced state for various values of  $J$ . As  $J$  decreases, the advantage of our construction becomes more evident, as expected. The improvement is also more visible at larger  $T$ , where higher-order cancellation in  $T$  becomes apparent. (See SM for additional simulations.)

*Conclusion.*— We introduced a high-order DD construction that suppresses arbitrary system–bath noise using only  $\mathcal{O}(|\mathcal{G}|K)$  pulses, canceling the leading system–bath coupling term  $J$  up to order  $K$  in the evolution time  $T$ . In the weak-coupling regime, where  $J$  is small and this term dominates the error, the sequence achieves the same leading order scaling as all other state-of-the-art DD sequences with substantially fewer pulses. Moreover, for  $n$ -qubit  $k$ -local noise with  $k = \mathcal{O}(1)$ , locality enables an exponential reduction in pulse count relative to conventional high-order DD, and the construction naturally extends to slow, time-dependent Hamiltonian noise.

To establish existence, we map pulse scheduling to the continuous necklace-splitting problem and, leveraging an efficient deterministic algorithm from that literature, show that a DD sequence using  $\mathcal{O}(|\mathcal{G}|K)$  pulses can be determined explicitly. We then constructed explicit  $3K$ -length pulse sequences through numerical optimization and verified their effectiveness via simulations, showing improvements over QDD. An interesting direction would be to implement this deterministic algorithm to generate and benchmark new DD sequences for large systems.

Our approach provides a practical route to extending qubit coherence times and may serve as a foundation for more resource-efficient pulse-sequence implementations in tasks such as quantum sensing, noise spectroscopy, and quantum simulation. More broadly, we hope that our work inspires further connections between quantum control and concrete mathematical problems, leading to more efficient and elegant protocol designs.

*Acknowledgments.*— This material is based upon work supported by the U.S. Department of Energy, Office of Science, Advanced Scientific Computing Research (ASCR), Express: 2023 Exploratory Research For Extreme-scale Science Program under Award Number DE-SC0024685. Additional support by the DOE Early Career Research Award No. DE-SC0026373 is acknowledged.

*Data Availability.*— The data that support the findings

of this article are openly available [64].

---

- [1] L. Viola, E. Knill, and S. Lloyd, Dynamical decoupling of open quantum systems, *Phys. Rev. Lett.* **82**, 2417 (1999).
- [2] E. L. Hahn, Spin echoes, *Phys. Rev.* **80**, 580 (1950).
- [3] S. Meiboom and D. Gill, Modified Spin-Echo Method for Measuring Nuclear Relaxation Times, *Rev. Sci. Instrum.* **29**, 688 (1958).
- [4] A. A. Maudsley, Modified Carr-Purcell-Meiboom-Gill sequence for NMR Fourier imaging applications, *Journal of Magnetic Resonance* **69**, 488 (1986).
- [5] L. Viola and E. Knill, Robust dynamical decoupling of quantum systems with bounded controls, *Phys. Rev. Lett.* **90**, 037901 (2003).
- [6] L. Viola and E. Knill, Random decoupling schemes for quantum dynamical control and error suppression, *Phys. Rev. Lett.* **94**, 060502 (2005).
- [7] K. Khodjasteh and D. A. Lidar, Fault-tolerant quantum dynamical decoupling, *Phys. Rev. Lett.* **95**, 180501 (2005).
- [8] K. Khodjasteh and D. A. Lidar, Performance of deterministic dynamical decoupling schemes: Concatenated and periodic pulse sequences, *Phys. Rev. A* **75**, 062310 (2007).
- [9] G. S. Uhrig, Keeping a quantum bit alive by optimized  $\pi$ -pulse sequences, *Phys. Rev. Lett.* **98**, 100504 (2007).
- [10] W. Yang and R.-B. Liu, Universality of uhrig dynamical decoupling for suppressing qubit pure dephasing and relaxation, *Phys. Rev. Lett.* **101**, 180403 (2008).
- [11] G. S. Uhrig, Concatenated control sequences based on optimized dynamic decoupling, *Phys. Rev. Lett.* **102**, 120502 (2009).
- [12] J. R. West, D. A. Lidar, B. H. Fong, and M. F. Gyure, High fidelity quantum gates via dynamical decoupling, *Phys. Rev. Lett.* **105**, 230503 (2010).
- [13] J. R. West, B. H. Fong, and D. A. Lidar, Near-optimal dynamical decoupling of a qubit, *Phys. Rev. Lett.* **104**, 130501 (2010).
- [14] G. S. Uhrig and D. A. Lidar, Rigorous bounds for optimal dynamical decoupling, *Phys. Rev. A* **82**, 012301 (2010).
- [15] Y. Xia, G. S. Uhrig, and D. A. Lidar, Rigorous performance bounds for quadratic and nested dynamical decoupling, *Phys. Rev. A* **84**, 062332 (2011).
- [16] H. K. Ng, D. A. Lidar, and J. Preskill, Combining dynamical decoupling with fault-tolerant quantum computation, *Phys. Rev. A* **84**, 012305 (2011).
- [17] Z.-Y. Wang and R.-B. Liu, Protection of quantum systems by nested dynamical decoupling, *Phys. Rev. A* **83**, 022306 (2011).
- [18] L. Jiang and A. Imambekov, Universal dynamical decoupling of multiqubit states from environment, *Phys. Rev. A* **84**, 060302 (2011).
- [19] G. Quiroz and D. A. Lidar, Optimized dynamical decoupling via genetic algorithms, *Physical Review A* **88**, 10.1103/physreva.88.052306 (2013).
- [20] A. D. Bookatz, M. Roetteler, and P. Wocjan, Improved bounded-strength decoupling schemes for local hamiltonians, *IEEE Transactions on Information Theory* **62**, 2881–2894 (2016).
- [21] G. T. Genov, D. Schraft, N. V. Vitanov, and T. Half

mann, Arbitrarily accurate pulse sequences for robust dynamical decoupling, *Phys. Rev. Lett.* **118**, 133202 (2017).

[22] C. Yi, L. Kim, and M. Marvian, Faster randomized dynamical decoupling, *Phys. Rev. Lett.* **136**, 010601 (2026).

[23] W. M. Witzel and S. Das Sarma, Concatenated dynamical decoupling in a solid-state spin bath, *Phys. Rev. B* **76**, 241303 (2007).

[24] M. J. Biercuk, H. Uys, A. P. VanDevender, N. Shiga, W. M. Itano, and J. J. Bollinger, Experimental uhlig dynamical decoupling using trapped ions, *Physical Review A* **79**, 10.1103/physreva.79.062324 (2009).

[25] M. J. Biercuk, H. Uys, A. P. VanDevender, N. Shiga, W. M. Itano, and J. J. Bollinger, Optimized dynamical decoupling in a model quantum memory, *Nature* **458**, 996 (2009).

[26] G. A. Álvarez, A. Ajoy, X. Peng, and D. Suter, Performance comparison of dynamical decoupling sequences for a qubit in a rapidly fluctuating spin bath, *Phys. Rev. A* **82**, 042306 (2010).

[27] G. de Lange, Z. H. Wang, D. Ristè, V. V. Dobrovitski, and R. Hanson, Universal dynamical decoupling of a single solid-state spin from a spin bath, *Science* **330**, 60 (2010).

[28] C. A. Ryan, J. S. Hodges, and D. G. Cory, Robust decoupling techniques to extend quantum coherence in diamond, *Phys. Rev. Lett.* **105**, 200402 (2010).

[29] C. Barthel, J. Medford, C. M. Marcus, M. P. Hanson, and A. C. Gossard, Interlaced dynamical decoupling and coherent operation of a singlet-triplet qubit, *Phys. Rev. Lett.* **105**, 266808 (2010).

[30] A. Ajoy, G. A. Álvarez, and D. Suter, Optimal pulse spacing for dynamical decoupling in the presence of a purely dephasing spin bath, *Phys. Rev. A* **83**, 032303 (2011).

[31] A. M. Souza, G. A. Álvarez, and D. Suter, Robust dynamical decoupling for quantum computing and quantum memory, *Phys. Rev. Lett.* **106**, 240501 (2011).

[32] J. Bylander, S. Gustavsson, F. Yan, F. Yoshihara, K. Harrabi, G. Fitch, D. G. Cory, Y. Nakamura, J.-S. Tsai, and W. D. Oliver, Noise spectroscopy through dynamical decoupling with a superconducting flux qubit, *Nat. Phys.* **7**, 565 (2011).

[33] J. Medford, L. Cywiński, C. Barthel, C. M. Marcus, M. P. Hanson, and A. C. Gossard, Scaling of dynamical decoupling for spin qubits, *Phys. Rev. Lett.* **108**, 086802 (2012).

[34] N. Zhao, S.-W. Ho, and R.-B. Liu, Decoherence and dynamical decoupling control of nitrogen vacancy center electron spins in nuclear spin baths, *Phys. Rev. B* **85**, 115303 (2012).

[35] X. Xu, Z. Wang, C. Duan, P. Huang, P. Wang, Y. Wang, N. Xu, X. Kong, F. Shi, X. Rong, and J. Du, Coherence-protected quantum gate by continuous dynamical decoupling in diamond, *Phys. Rev. Lett.* **109**, 070502 (2012).

[36] D. Farfurnik, A. Jarmola, L. M. Pham, Z. H. Wang, V. V. Dobrovitski, R. L. Walsworth, D. Budker, and N. Bar-Gill, Optimizing a dynamical decoupling protocol for solid-state electronic spin ensembles in diamond, *Phys. Rev. B* **92**, 060301 (2015).

[37] B. Pokharel, N. Anand, B. Fortman, and D. A. Lidar, Demonstration of fidelity improvement using dynamical decoupling with superconducting qubits, *Phys. Rev. Lett.* **121**, 220502 (2018).

[38] V. Tripathi, H. Chen, M. Khezri, K.-W. Yip, E. Levenson-Falk, and D. A. Lidar, Suppression of crosstalk in superconducting qubits using dynamical decoupling, *Phys. Rev. Appl.* **18**, 024068 (2022).

[39] N. Ezzell, B. Pokharel, L. Tewala, G. Quiroz, and D. A. Lidar, Dynamical decoupling for superconducting qubits: A performance survey, *Phys. Rev. Appl.* **20**, 064027 (2023).

[40] Y. Kim, C. J. Wood, T. J. Yoder, S. T. Merkel, J. M. Gambetta, K. Temme, and A. Kandala, Scalable error mitigation for noisy quantum circuits produces competitive expectation values, *Nat. Phys.* **19**, 752 (2023).

[41] R. Acharya, D. A. Abanin, L. Aghababaie-Beni, I. Aleiner, T. I. Andersen, *et al.*, Quantum error correction below the surface code threshold, *Nature* **638**, 920 (2025).

[42] D. Bluvstein, S. J. Evered, A. A. Geim, S. H. Li, H. Zhou, T. Manovitz, S. Ebadi, M. Cain, M. Kalinowski, D. Hangleiter, J. P. Bonilla Ataides, N. Maskara, I. Cong, X. Gao, P. Sales Rodriguez, T. Karolyshyn, G. Semeghini, M. J. Gullans, M. Greiner, V. Vuletić, and M. D. Lukin, Logical quantum processor based on reconfigurable atom arrays, *Nature* **626**, 58 (2024).

[43] A. Paetznick, M. P. da Silva, C. Ryan-Anderson, J. M. Bello-Rivas, J. P. C. III, A. Chernoguzov, J. M. Dreiling, C. Foltz, F. Frachon, J. P. Gaebler, T. M. Gatterman, L. Grans-Samuelsson, D. Gresh, D. Hayes, N. Hewitt, C. Holliman, C. V. Horst, J. Johansen, D. Lucchetti, Y. Matsuoka, M. Mills, S. A. Moses, B. Neyenhuis, A. Paz, J. Pino, P. Siegfried, A. Sundaram, D. Tom, S. J. Wernli, M. Zanner, R. P. Stutz, and K. M. Svore, *Demonstration of logical qubits and repeated error correction with better-than-physical error rates* (2024), arXiv:2404.02280 [quant-ph].

[44] D. Bluvstein, A. A. Geim, S. H. Li, S. J. Evered, J. P. B. Ataides, G. Baranes, A. Gu, T. Manovitz, M. Xu, M. Kalinowski, S. Majidy, C. Kokail, N. Maskara, E. C. Trapp, L. M. Stewart, S. Hollerith, H. Zhou, M. J. Gullans, S. F. Yelin, M. Greiner, V. Vuletić, M. Cain, and M. D. Lukin, *Architectural mechanisms of a universal fault-tolerant quantum computer* (2025), arXiv:2506.20661 [quant-ph].

[45] A. Vezvaei, C. Benito, M. Morford-Oberst, A. Bermudez, and D. A. Lidar, *Surface code scaling on heavy-hex superconducting quantum processors* (2025), arXiv:2510.18847 [quant-ph].

[46] B. M. Terhal and G. Burkard, Fault-tolerant quantum computation for local non-markovian noise, *Phys. Rev. A* **71**, 012336 (2005).

[47] D. Aharonov, A. Kitaev, and J. Preskill, Fault-tolerant quantum computation with long-range correlated noise, *Phys. Rev. Lett.* **96**, 050504 (2006).

[48] U. von Lüpke, F. Beaudoin, L. M. Norris, Y. Sung, R. Winik, J. Y. Qiu, M. Kjaergaard, D. Kim, J. Yoder, S. Gustavsson, L. Viola, and W. D. Oliver, Two-qubit spectroscopy of spatiotemporally correlated quantum noise in superconducting qubits, *PRX Quantum* **1**, 010305 (2020).

[49] H.-P. Breuer and F. Petruccione, *The theory of open quantum systems* (OUP Oxford, 2002).

[50] L. Viola, S. Lloyd, and E. Knill, Universal control of decoupled quantum systems, *Phys. Rev. Lett.* **83**, 4888 (1999).

[51] D. A. Lidar, Towards fault tolerant adiabatic quantum computation, *Phys. Rev. Lett.* **100**, 160506 (2008).

- [52] K. Khodjasteh and D. A. Lidar, Rigorous bounds on the performance of a hybrid dynamical-decoupling quantum-computing scheme, *Physical Review A* **78**, 10.1103/phys-reva.78.012355 (2008).
- [53] G. Quiroz and D. A. Lidar, High-fidelity adiabatic quantum computation via dynamical decoupling, *Phys. Rev. A* **86**, 042333 (2012).
- [54] A. De and L. P. Pryadko, Universal set of scalable dynamically corrected gates for quantum error correction with always-on qubit couplings, *Phys. Rev. Lett.* **110**, 070503 (2013).
- [55] C. L. Degen, F. Reinhard, and P. Cappellaro, Quantum sensing, *Rev. Mod. Phys.* **89**, 035002 (2017).
- [56] N. Alon, Splitting necklaces, *Advances in Mathematics* **63**, 247 (1987).
- [57] N. Alon and A. Graur, Efficient Splitting of Necklaces, in *48th International Colloquium on Automata, Languages, and Programming (ICALP 2021)*, Leibniz International Proceedings in Informatics (LIPIcs), Vol. 198, edited by N. Bansal, E. Merelli, and J. Worrell (Schloss Dagstuhl – Leibniz-Zentrum für Informatik, Dagstuhl, Germany, 2021) pp. 14:1–14:17.
- [58] W. Magnus, On the exponential solution of differential equations for a linear operator, *Communications on Pure and Applied Mathematics* **7**, 649 (1954).
- [59] S. Blanes, F. Casas, J. Oteo, and J. Ros, The magnus expansion and some of its applications, *Physics Reports* **470**, 151–238 (2009).
- [60] P. Zanardi, Symmetrizing evolutions, *Physics Letters A* **258**, 77–82 (1999).
- [61] A. Filos-Ratsikas, S. K. S. Frederiksen, P. W. Goldberg, and J. Zhang, Hardness results for consensus-halving (2018), [arXiv:1609.05136 \[cs.GT\]](https://arxiv.org/abs/1609.05136).
- [62] T. J. Green, J. Sastrawan, H. Uys, and M. J. Biercuk, Arbitrary quantum control of qubits in the presence of universal noise, *New Journal of Physics* **15**, 095004 (2013).
- [63] G. Ramon and L. Cywiński, Qubit decoherence under two-axis coupling to low-frequency noises, *Phys. Rev. B* **105**, L041303 (2022).
- [64] L. Kim and M. Marvian, High-order dynamical decoupling for arbitrary noise in the weak-coupling regime, <https://github.com/Leeseok-628/high-order-dd-weak-coupling> (2026), GitHub repository.

## Supplemental Material

### I. PROOF OF THEOREM 1

**Theorem S1** (Existence of an order- $K$  moment-cancelling sequence with at most  $(|\mathcal{G}| - 1)K$  pulses; Restatement of Theorem 1). *Let  $H = H_0 + H_{SB}$  with  $H_{SB} = \sum_{\alpha} \sigma_{\alpha} \otimes B_{\alpha}$  and let  $\mathcal{G}$  be a decoupling group for  $H$  as defined in Eq. (14). For any integer  $K \geq 1$ , there exist piecewise-constant functions  $y_{\alpha} : [0, 1] \rightarrow \{\pm 1\}$ , indexed by all Pauli strings  $\sigma_{\alpha}$  appearing in  $H_{SB}$ , such that:*

1. *there exist (normalized) pulse timings  $0 < \tau_1 < \dots < \tau_L < 1$  with*

$$L \leq (|\mathcal{G}| - 1)K \quad (\text{S1})$$

*for which all  $y_{\alpha}(\tau)$  are constant on each subinterval  $[0, \tau_1], [\tau_1, \tau_2], \dots, [\tau_L, 1]$ , and*

2. *the generalized moments in (12) vanish,*

$$M_{\alpha, m} = \int_0^1 y_{\alpha}(\tau) \tau^m d\tau = 0, \quad (\text{S2})$$

*for all  $\alpha$  and all  $m = 0, 1, \dots, K - 1$ .*

Our construction hinges on the continuous necklace-splitting theorem:

**Lemma S2** (Necklace-splitting for continuous densities, Theorem 1.2 in [56]). *Let  $f_1, \dots, f_K : [0, 1] \rightarrow [0, \infty)$  be continuous functions and fix an integer  $q \geq 2$ . There exist cut points  $0 < \tau_1 < \dots < \tau_L < 1$  with  $L \leq (q - 1)K$  and a partition of the subintervals  $[0, \tau_1], [\tau_1, \tau_2], \dots, [\tau_L, 1]$  into  $q$  bins  $A_1, \dots, A_q$  such that, for every  $j = 1, \dots, K$  and  $c = 1, \dots, q$ ,*

$$\int_{A_c} f_j(\tau) d\tau = \frac{1}{q} \int_0^1 f_j(\tau) d\tau. \quad (\text{S3})$$

We note that the original theorem is stated for finite measures. Restricting to absolutely continuous measures  $d\mu_j(\tau) = f_j(\tau) d\tau$  immediately gives the above statement.

To prove Theorem S1, apply Lemma S2 with  $q = |\mathcal{G}|$  and  $f_m(\tau) = \tau^m$  for  $m = 0, \dots, K - 1$ , and map the  $q$  bins to elements of  $\mathcal{G}$ .

*Proof of Theorem S1.* For each Pauli string  $\sigma_{\alpha}$  in  $H_{SB}$  and each  $g \in \mathcal{G}$ , conjugation yields

$$g_{\ell}^{\dagger} \sigma_{\alpha} g_{\ell} = \chi_{\alpha}(g_{\ell}) \sigma_{\alpha}, \quad \chi_{\alpha}(g_{\ell}) \in \{\pm 1\}. \quad (\text{S4})$$

By expanding  $H_{SB} = \sum_{\alpha} \sigma_{\alpha} \otimes B_{\alpha}$  and using the decoupling group condition (14),

$$0 = \frac{1}{|\mathcal{G}|} \sum_{g \in \mathcal{G}} g^{\dagger} H_{SB} g = \frac{1}{|\mathcal{G}|} \sum_{\ell=1}^{|\mathcal{G}|} \sum_{\alpha} g_{\ell}^{\dagger} \sigma_{\alpha} g_{\ell} \otimes B_{\alpha} \quad (\text{S5})$$

$$= \sum_{\alpha} \left( \frac{1}{|\mathcal{G}|} \sum_{\ell=1}^{|\mathcal{G}|} \chi_{\alpha}(g_{\ell}) \right) \sigma_{\alpha} \otimes B_{\alpha}, \quad (\text{S6})$$

we see that

$$\sum_{\ell=1}^{|\mathcal{G}|} \chi_{\alpha}(g_{\ell}) = 0. \quad (\text{S7})$$

Next, apply Lemma S2 with  $q = |\mathcal{G}|$  and the  $K$  nonnegative continuous functions  $f_m(\tau) = \tau^m$  ( $m = 0, 1, \dots, K - 1$ ). The lemma guarantees the existence of cut points  $0 < \tau_1 < \dots < \tau_L < 1$ , with  $L \leq (|\mathcal{G}| - 1)K$  and a partition of the induced subintervals into bins  $A_1, \dots, A_{|\mathcal{G}|}$  such that for all  $m < K$  and all  $c$ ,

$$\int_{A_c} \tau^m d\tau = \frac{1}{q} \int_0^1 \tau^m d\tau. \quad (\text{S8})$$

Define  $y_\alpha(\tau)$  by assigning to each bin  $A_c$  the sign pattern determined by  $g_c$

$$y_\alpha(\tau) \equiv \chi_\alpha(g_c) \quad \text{for } \tau \in A_c. \quad (\text{S9})$$

By construction, each  $y_\alpha$  is piecewise constant and is constant on every subinterval of the partition  $[0, \tau_1), [\tau_1, \tau_2), \dots, [\tau_L, 1]$ , which satisfies Condition (1).

It remains to verify the generalized moment constraints in Condition (2). For every  $\alpha$  and  $m < K$ ,

$$M_{\alpha, m} = \int_0^1 y_\alpha(\tau) \tau^m d\tau \quad (\text{S10})$$

$$= \sum_{c=1}^{|\mathcal{G}|} \chi_\alpha(g_c) \int_{A_c} \tau^m d\tau \quad (\text{S11})$$

$$= \frac{1}{|\mathcal{G}|} \left( \sum_{c=1}^{|\mathcal{G}|} \chi_\alpha(g_c) \right) \int_0^1 \tau^m d\tau, \quad (\text{S12})$$

$$= 0, \quad (\text{S13})$$

where we used Eq. (S8) and Eq. (S7). By Lemma S2, the number of cut points (and hence the number of pulses) is at most  $L \leq (|\mathcal{G}| - 1)K$ , and the number of constant segments is at most  $L + 1 \leq (|\mathcal{G}| - 1)K + 1$ . This completes the proof.  $\square$

## II. PROOF OF LEMMA 2

**Lemma S3** ( $\Omega(K)$  lower bound; Restatement of Lemma 2). *Let  $y : [0, 1] \rightarrow \{\pm 1\}$  be piecewise constant with  $r$  sign changes on  $(0, 1)$ . If*

$$\int_0^1 y(\tau) \tau^m d\tau = 0 \quad (m = 0, 1, \dots, K-1), \quad (\text{S14})$$

*then necessarily  $r \geq K$ .*

The idea of the proof is as follows. Since Eq. (S14) means that  $y$  is orthogonal to every polynomial with degree  $r$ , it suffices to find a single polynomial  $q$  with  $\deg q \leq r$  such that  $\int_0^1 y(\tau) q(\tau) d\tau \neq 0$ . By choosing a polynomial  $P$  that vanishes at all sign-flip points and setting  $q := P'$ , the integral  $\int_0^1 y(\tau) P'(\tau) d\tau$  telescopes to an endpoint term  $P(1)$ , which we can set to be nonzero. This yields the desired contradiction.

*Proof.* Let the sign-flipping points be  $0 < \tau_1 < \dots < \tau_r < 1$ , and set  $\tau_0 \equiv 0$ ,  $\tau_{r+1} \equiv 1$ . Let  $s_k \in \{\pm 1\}$  be the constant value of  $y$  on  $(\tau_k, \tau_{k+1})$  for  $k = 0, \dots, r$ . Define

$$P(\tau) = a\tau \prod_{j=1}^r (\tau - \tau_j), \quad a \equiv \frac{s_r}{\prod_{j=1}^r (1 - \tau_j)}. \quad (\text{S15})$$

Then  $P(\tau_j) = 0$  for  $j = 1, \dots, r$ ,  $P(0) = 0$ , and  $P(1) = s_r$ . We choose  $q(\tau) = P'(\tau)$ ; note that  $\deg P = r + 1$  and  $\deg q \leq r$ .

We compute

$$\int_0^1 y(\tau) P'(\tau) d\tau = \sum_{k=0}^r s_k \int_{\tau_k}^{\tau_{k+1}} P'(\tau) d\tau \quad (\text{S16})$$

$$= \sum_{k=0}^r s_k (P(\tau_{k+1}) - P(\tau_k)). \quad (\text{S17})$$

Rearranging the sum gives

$$\sum_{k=0}^r s_k (P(\tau_{k+1}) - P(\tau_k)) \quad (\text{S18})$$

$$= s_r P(1) - s_0 P(0) - \sum_{j=1}^r (s_j - s_{j-1}) P(\tau_j) \quad (\text{S19})$$

$$= 1, \quad (\text{S20})$$

where the last equality holds as (by construction)  $P(\tau_j) = 0$  for all  $j$  and  $P(0) = 0$ , while  $P(1) = s_r$ .

If  $r \leq K - 1$  then  $\deg P' \leq K - 1$ , so we can write  $P'(\tau) = \sum_{m=0}^{K-1} a_m \tau^m$  and thus

$$\int_0^1 y(\tau) P'(\tau) d\tau = \sum_{m=0}^{K-1} a_m \int_0^1 y(\tau) \tau^m d\tau = 0, \quad (\text{S21})$$

which contradicts the previous equality. Therefore  $r \geq K$ .  $\square$

### III. EXTENSION TO TIME-DEPENDENT (CLASSICAL) NOISE

In this section, we briefly note that the same moment-cancellation mechanism extends to time-dependent (classical) Hamiltonian noise models that are widely used to describe environmental fluctuations, and for which DD performance has been extensively studied (see, e.g., Refs. [26, 31, 32, 62, 63]). For concreteness, consider a single qubit with

$$H(t) = H_c(t) + H_n(t), \quad H_n(t) = \sum_{\alpha \in \{x,y,z\}} \beta_{\alpha}(t) \sigma_{\alpha}, \quad (\text{S22})$$

where  $\beta_{\alpha}(t) \in \mathbb{R}$  are unknown time-dependent coefficients and  $H_c(t)$  implements ideal instantaneous Pauli pulses. Let  $U_c(t)$  be the ideal control propagator generated by  $H_c(t)$ , and write the toggling-frame evolution as  $\tilde{U}(T) = \mathcal{T} \exp \left[ -i \int_0^T \tilde{H}_n(t) dt \right]$  with  $\tilde{H}_n(t) := U_c^\dagger(t) H_n(t) U_c(t)$ . For Pauli pulses, conjugation maps each Pauli to itself up to a sign on every free-evolution segment, so

$$\tilde{H}_n(t) = \sum_{\alpha} y_{\alpha}(t) \beta_{\alpha}(t) \sigma_{\alpha}, \quad y_{\alpha}(t) \in \{\pm 1\}. \quad (\text{S23})$$

Expanding  $\tilde{U}(T)$  via the Magnus series, the leading term is

$$\Omega_1(T) = -i \int_0^T \tilde{H}_n(t) dt = -i \sum_{\alpha} \sigma_{\alpha} \int_0^T y_{\alpha}(t) \beta_{\alpha}(t) dt. \quad (\text{S24})$$

We can Taylor expand  $\beta_{\alpha}(T\tau)$  in normalized time  $\tau = t/T$ . Assuming  $\beta_{\alpha}$  is  $K$ -times differentiable on  $[0, T]$ , Taylor's theorem gives

$$\beta_{\alpha}(T\tau) = \sum_{m=0}^{K-1} \frac{\beta_{\alpha}^{(m)}(0)}{m!} (T\tau)^m + \frac{(T\tau)^K}{K!} \beta_{\alpha}^{(K)}(\xi_{\alpha,\tau}), \quad \xi_{\alpha,\tau} \in [0, T\tau]. \quad (\text{S25})$$

Substituting (S25) into (S24) shows that the coefficients of  $T^{m+1}$  are proportional to the same generalized moments as in the main text,

$$M_{\alpha,m} = \int_0^1 y_{\alpha}(\tau) \tau^m d\tau, \quad (\text{S26})$$

so imposing  $M_{\alpha,m} = 0$  for all  $\alpha$  and  $m = 0, \dots, K - 1$  cancels all contributions to  $\Omega_1(T)$  up to order  $K$ .

Define the noise-amplitude scale

$$\beta_{\max} := \sup_{t \in [0, T]} \sum_{\alpha \in \{x, y, z\}} |\beta_{\alpha}(t)|, \quad (\text{S27})$$

so that  $\|\tilde{H}_n(t)\| \leq \beta_{\max}$  for all  $t$ . In addition, in the slow (low-bandwidth) regime we assume that  $\beta_\alpha$  has an effective cutoff frequency  $\omega_c$ , in the sense that

$$\sup_{t \in [0, T]} |\beta_\alpha^{(K)}(t)| = \mathcal{O}(\beta_{\max} \omega_c^K). \quad (\text{S28})$$

For example, consider a single-frequency noise  $\beta_\alpha(t) = A_\alpha \cos(\omega t + \phi_\alpha)$ . Then  $\sup_{t \in [0, T]} |\beta_\alpha(t)| = |A_\alpha|$  and  $\sup_{t \in [0, T]} |\beta_\alpha^{(K)}(t)| = |A_\alpha| |\omega|^K$ . If  $|\omega| \leq \omega_c$  and  $|A_\alpha| \leq \beta_{\max}$ , it follows that  $\sup_{t \in [0, T]} |\beta_\alpha^{(K)}(t)| = \mathcal{O}(\beta_{\max} \omega_c^K)$  as in (S28).

Then the Taylor remainder term in (S25) implies

$$\|\Omega_1(T)\| = \mathcal{O}(\beta_{\max} T (\omega_c T)^K). \quad (\text{S29})$$

The second-order Magnus expansion is bounded by

$$\|\Omega_2(T)\| = \mathcal{O}(\beta_{\max}^2 T^2). \quad (\text{S30})$$

Hence, in the small  $\beta_{\max}, T$  regime where the Magnus expansion converges,

$$\|\tilde{U}(T) - I\| = \mathcal{O}(\beta_{\max} T (\omega_c T)^K) + \mathcal{O}(\beta_{\max}^2 T^2), \quad (\text{S31})$$

which matches the structure of the main text estimate in Eq. (6), with the system-bath coupling scale replaced by the classical noise amplitude scale.

## IV. NUMERICAL SIMULATION DETAILS AND ADDITIONAL SIMULATIONS

### A. Numerical optimization procedure

In the single-qubit example in the main text, the goal is to construct a Pauli pulse sequence that satisfies the moment constraints up to order  $K - 1$  while using only  $3K$  (+1) pulses. We fix a pulse pattern a priori and optimize only the inter-pulse intervals.

For a given order  $K$ , we fix the number of inter-pulse intervals to be  $L = 3K + 1$  and choose a fixed sequence of control pulses  $X \rightarrow Z \rightarrow X \rightarrow Z \rightarrow \dots$ . This generates control frames  $f_1, \dots, f_L \in G = \{I, X, Y, Z\}$ . Each frame  $f_\ell$  is associated with a “sign triple”

$$\mathbf{s}_\ell = (s_{\ell,x}, s_{\ell,y}, s_{\ell,z}) \in \{\pm 1\}^3, \quad \ell = 1, \dots, L, \quad (\text{S32})$$

which specifies the sign of the Pauli operators  $\sigma_\alpha$  in the toggling frame during the  $\ell$ -th interval. Equivalently, this defines switching functions  $y_\alpha(\tau)$  for  $\alpha \in \{x, y, z\}$  that are piecewise constant on  $[0, 1]$ :  $y_\alpha(\tau) = s_{\ell,\alpha}$  for  $\tau \in [t_{\ell-1}, t_\ell]$ , where  $0 = t_0 < t_1 < \dots < t_L = 1$  are the normalized segment boundaries.

Rather than performing any numerical quadrature, we evaluate the integrals analytically. Since  $y_\alpha(\tau)$  is piecewise constant,

$$\int_0^1 \tau^m y_\alpha(\tau) d\tau = \sum_{\ell=1}^L s_{\ell,\alpha} \int_{t_{\ell-1}}^{t_\ell} \tau^m d\tau = \frac{1}{m+1} \sum_{\ell=1}^L s_{\ell,\alpha} (t_\ell^{m+1} - t_{\ell-1}^{m+1}), \quad (\text{S33})$$

and the overall factor  $1/(m+1)$  is irrelevant for the location of the zeros. We therefore collect all moment residuals into a single vector  $r(\Delta\tau) \in \mathbb{R}^{3K}$  whose components are

$$r_{\alpha,m}(\Delta\tau) = \sum_{\ell=1}^L s_{\ell,\alpha} (t_\ell^{m+1} - t_{\ell-1}^{m+1}), \quad \alpha \in \{x, y, z\}, \quad m = 0, \dots, K-1, \quad (\text{S34})$$

and minimize the squared norm

$$\Phi(\Delta\tau) = \sum_{\alpha,m} |r_{\alpha,m}(\Delta\tau)|^2, \quad (\text{S35})$$

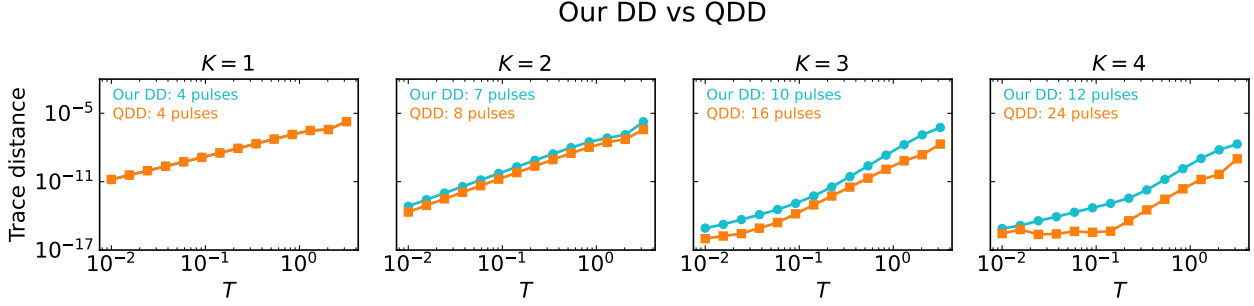


FIG. S1: Comparison between our order- $K$  decoupling sequence and QDD in the same single-qubit model used in the main text with  $\beta = 1$  and  $J = 10^{-5}$ . The plot shows the trace-distance error between the actual and ideal system states as a function of total evolution time  $T$ .

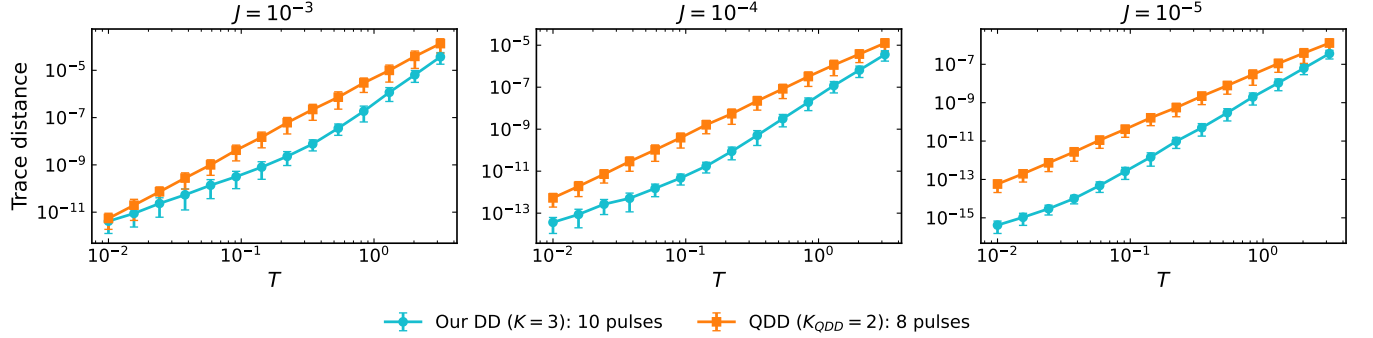


FIG. S2: Comparison between our DD sequences and QDD for the single-qubit general decoherence model. We show the average trace distance error of the reduced system state versus  $T$  for several small coupling strengths  $J$ , comparing our  $K = 3$  DD (10 pulses) with QDD at  $K_{\text{QDD}} = 2$  (8 pulses). Each data point is averaged over 100 random initial product states.

subject to  $\Delta\tau_\ell > 0$  and  $\sum_\ell \Delta\tau_\ell = 1$ . Up to an overall constant, the objective (S35) is equivalent to the cost function defined in (23) of the main text.

To enforce the simplex constraint, we parameterize the intervals by an unconstrained vector  $\theta \in \mathbb{R}^L$  via a softmax map,

$$\Delta\tau_\ell(\theta) = \frac{e^{\theta_\ell}}{\sum_{j=1}^L e^{\theta_j}}, \quad \ell = 1, \dots, L, \quad (\text{S36})$$

and treat  $r(\theta) := r(\Delta\tau(\theta))$  as a nonlinear map  $\mathbb{R}^L \rightarrow \mathbb{R}^{3K}$ . The optimization problem is then formulated as a nonlinear least-squares problem for  $\theta$ , which we solve with a standard (trust-region reflective) algorithm. Specifically, we use the `least_squares` function from `SciPY`. We use stopping tolerances on the function value, step size, and gradient (`ftol = xtol = gtol = 10^-15`) and allow up to `max_nfev = 10^5 := N_{\text{fev}}` function evaluations per run.

For a given order  $K$ , the nonlinear least-squares problem has  $3K + 1$  variables and  $3K$  residuals. Each evaluation of the moment residual vector  $r(\theta)$  costs  $\mathcal{O}(K^2)$  operations, and the trust-region reflective solver uses at most  $N_{\text{fev}}$  function evaluations per run. The total classical computational cost therefore scales as  $\mathcal{O}(N_{\text{fev}}K^2)$ . In general, if one chooses to apply the same numerical optimization to a DD sequence constructed from a decoupling group  $\mathcal{G}$  with  $\mathcal{O}(|\mathcal{G}|K)$  segments, the classical computational cost scales as  $\mathcal{O}(N_{\text{fev}}(|\mathcal{G}|K)^2)$ .

## B. Comparison with QDD: additional simulations

In the main text, we benchmarked our construction against Quadratic Dynamical Decoupling (QDD) [13]. QDD is obtained by nesting two single-axis Uhrig sequences along orthogonal control axes (here taken to be  $X$  and  $Z$ ), and suppresses arbitrary single-qubit noise to order  $K_{\text{QDD}}$  using at most  $(K_{\text{QDD}} + 1)^2$  pulses. QDD is widely considered to be (nearly) optimal for suppressing single-qubit noise.

In this section, we provide additional simulations on the comparison for various orders  $K$ . We use the same numerical setup as the numerical section in the main text, with the weak-coupling parameters fixed to  $\beta = 1$  and  $J = 10^{-5}$ . We choose the initial state  $|+\rangle$  for both the system and the bath, evolve under the noisy dynamics with a given DD sequence, and compute the trace distance between the reduced system state and the ideal state obtained in the absence of system-bath coupling. This error is plotted as a function of the total evolution time  $T$ . Figure S1 shows results for  $K = K_{\text{QDD}} = 1, 2, 3, 4$ . Our DD sequence achieves the expected error scaling using only  $3K(+1)$  pulses, compared to  $(K_{\text{QDD}} + 1)^2$  pulses for QDD.

Finally, in addition to the comparisons presented in the main text (Fig. 3), we benchmark performance at a comparable resource budget by comparing our sequence ( $K = 3, 10$  pulses) with a QDD sequence of similar pulse count ( $K_{\text{QDD}} = 2, 8$  pulses) under the same setup. Although our protocol uses two additional pulses, our protocol achieves lower trace distance across all tested ranges of  $T$  and  $J$ , as shown in Fig. S2.

## C. Extended data of optimized pulse timings and effect of imprecise pulse timing

TABLE S1: Normalized segment lengths obtained by minimizing  $\Phi(\Delta\tau)$ . The pulse sequence is  $X \rightarrow Z \rightarrow X \rightarrow Z \dots$ . Values are shown to 15 decimal places.

$K$	$\{\Delta\tau_i\}_{i=1}^L$
1	[0.2500000000000000, 0.2500000000000000, 0.2500000000000000, 0.2500000000000000]
2	[0.078464834591372, 0.1249999999999999, 0.171535165408626, 0.2500000000000001, 0.171535165408628, 0.1250000000000001, 0.078464834591374]
3	[0.032292826653268, 0.063198676159276, 0.098322279339589, 0.151677720660432, 0.154508497187470, 0.154508497187474, 0.151677720660411, 0.098322279339567, 0.063198676159263, 0.032292826653251]
4	[0.015740558567996, 0.034840993778921, 0.058326727422055, 0.092639337921122, 0.109259441431874, 0.122519668299637, 0.133346545155644, 0.122519668299808, 0.109259441431969, 0.092639337921442, 0.058326727422301, 0.034840993779070, 0.015740558568160]
5	[0.008599239338160, 0.020714620114750, 0.036488791784096, 0.059197348763041, 0.075300583772990, 0.089748095447975, 0.103048492653219, 0.106902828125843, 0.106902828125842, 0.103048492653202, 0.089748095447950, 0.075300583772968, 0.059197348763007, 0.036488791784073, 0.020714620114735, 0.008599239338148]
6	[0.005099840472689, 0.013081296294727, 0.023951104697432, 0.039541779209467, 0.052702696284812, 0.065297618986759, 0.077549425157617, 0.085458220790868, 0.09069693338149, 0.093242169437664, 0.090696933387990, 0.085458220790698, 0.077549425157258, 0.065297618986355, 0.052702696284446, 0.039541779208967, 0.023951104697093, 0.013081296294494, 0.005099840472515]
7	[0.003218107155529, 0.008668617548996, 0.016370484427467, 0.027437910209365, 0.037772854809786, 0.048100983157502, 0.058499818469824, 0.066844362503103, 0.073589329135886, 0.078650108193099, 0.080847424390996, 0.080847424390950, 0.078650108192911, 0.073589329135586, 0.066844362502754, 0.058499818469383, 0.048100983157064, 0.037772854809394, 0.027437910208959, 0.016370484427200, 0.008668617548824, 0.003218107155422]
8	[0.002131868452877, 0.005973589234768, 0.011573393450091, 0.019658348833883, 0.027726790026254, 0.036051120042435, 0.044640380218587, 0.052270651341861, 0.059000709140531, 0.064723118015122, 0.068786226300013, 0.071323172469493, 0.072281264701016, 0.071323172476857, 0.068786226312206, 0.064723118034568, 0.059000709164710, 0.052270651368313, 0.044640380249883, 0.036051120072752, 0.027726790054342, 0.019658348862506, 0.011573393469221, 0.005973589247443, 0.002131868460270]

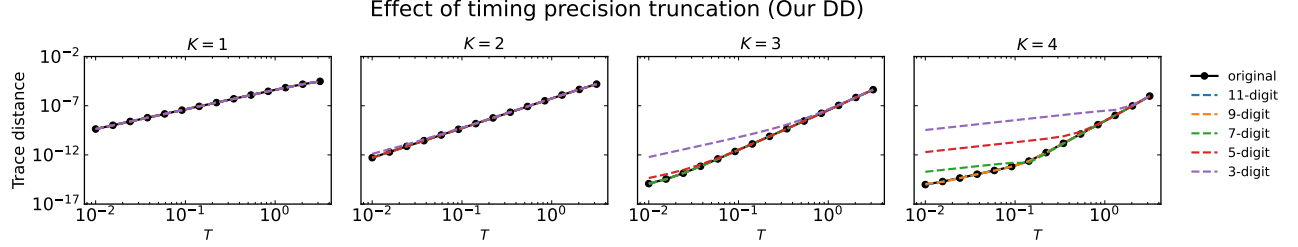


FIG. S3: Error vs.  $T$  for our DD sequence with various digit truncations.

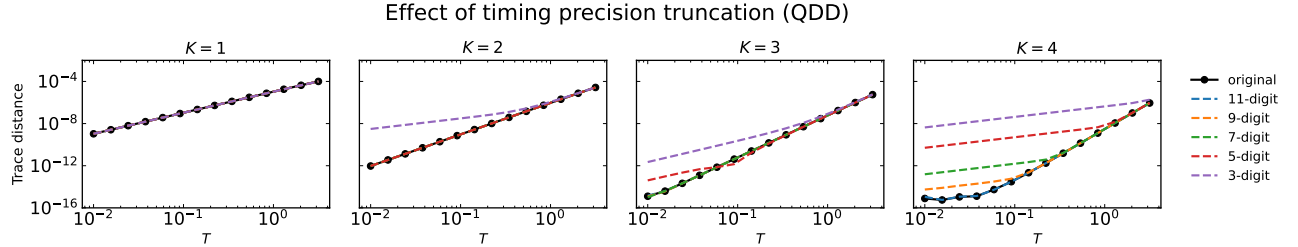


FIG. S4: Same analysis as Fig. S3 for QDD, showing consistent  $T_c$  behavior.

In Table S1, we provide precise values of the pulse intervals up to  $K = 8$ .

In practice, the pulse timings of the sequence shown in Table S1 may not be implemented exactly, but can include some perturbations. Let  $0 = \tau_0 < \tau_1 < \dots < \tau_L = 1$  be the ideal (normalized) pulse times, and model the implemented times as

$$\tilde{\tau}_k = \tau_k + \delta\tau_k, \quad |\delta\tau_k| \leq \varepsilon, \quad (\text{S37})$$

where  $\varepsilon$  describes the timing precision.

In physical time  $t \in [0, T]$  the ideal pulses are applied at  $t_k = \tau_k T$ , and the corresponding toggling-frame Hamiltonian  $\tilde{H}(t)$  is piecewise constant, changing only at the switching times. With timing errors the pulses are applied at  $\tilde{t}_k = \tilde{\tau}_k T$ , giving an implemented Hamiltonian  $\tilde{H}_\varepsilon(t)$ . A straightforward calculation then yields

$$\|\tilde{U}_\varepsilon(T) - \tilde{U}(T)\| \leq \int_0^T \|\tilde{H}_\varepsilon(t) - \tilde{H}(t)\| dt = \mathcal{O}(J\varepsilon LT), \quad (\text{S38})$$

where  $\tilde{U}(T)$  and  $\tilde{U}_\varepsilon(T)$  denote the ideal and implemented evolution operators in the toggling frame. This argument only uses the piecewise-constant structure of the control, and therefore applies generically to dynamical decoupling sequences.

To check this, we perform numerical simulations (with the same setups as in Section IV B), but now truncate the decimal digits of the optimized pulse timings in Table S1, as well as for QDD. For fixed  $J, K$ , and a given number  $d$  of kept decimal digits, we vary  $T$ . A simple estimate suggests that the crossover time  $T_c$  at which the truncated sequence starts to deviate from the ideal (full-precision) error curve is determined by

$$JT_c^{K+1} \sim J\varepsilon LT_c, \quad (\text{S39})$$

where  $L$  is the number of pulses and  $\varepsilon$  is the typical timing error induced by truncation. This gives

$$T_c \sim (\varepsilon L)^{1/K}, \quad (\text{S40})$$

so that if  $\varepsilon$  scales as  $10^{-d}$ , we expect  $T_c \propto 10^{-d/K}$ . This scaling behavior is consistent with the numerical results shown in Figs. S3 and S4, where the deviation point between the truncated and ideal curves moves systematically as the number of retained digits is increased.